



Exploring the effects of Pb substitution on the structure, magnetic, and magnetocaloric properties of $\text{La}_{1.96}\text{Pb}_{0.04}\text{NiMnO}_6$

Arda Kandemir^{1*}  Ali Osman Ayaş²  Ahmet Ekicibil¹ 

¹Çukurova University, Faculty of Science and Letters, Department of Physics, Adana, Türkiye.

²Adıyaman University, Faculty of Science and Letters, Department of Physics, Adıyaman, Türkiye.

ABSTRACT

Providing energy demands while caring for the environment and dealing with a decrease in natural energy resources are major challenges of our time. The greenhouse gas emissions worsen the situation in terms of health risks and put pressure on scientists to urgently seek solutions. As green technologies offer hopeful solutions to these demanding problems, they are getting attention. Refrigeration's noteworthy energy consumption makes it a prime target for efficiency developments compared to other technologies. To address concerns about energy consumption, researchers are exploring improvements in conventional cooling technologies. Magnetic cooling systems impress with their energy efficiency, affordability, and green technology, making them strong candidates for replacing current cooling systems. Research on MC emphasizes the importance of selecting coolants with high magnetic entropy. These materials experience a larger temperature variation under a low external magnetic field, making them more efficient. Magnetic refrigeration holds great potential, but research efforts continue to optimize the materials for even better performance, as shown by the literature. Growing on current research, this study analyses the characteristic features of $\text{La}_{1.96}\text{Pb}_{0.04}\text{NiMnO}_6$ double perovskite material. The sol-gel technique was used to synthesize the compound, followed by X-ray Diffraction analysis at room temperature to determine its crystal structure. Additionally, we used Scanning Electron Microscopy with Energy-Dispersive X-ray Spectroscopy to investigate the compound's morphology and elemental composition. Temperature-dependent magnetization and magnetic field-dependent magnetization analyses were taken to investigate the magnetic behavior of the compound. Temperature-dependent magnetization analysis revealed that a magnetic phase transition from the ferromagnetic to the paramagnetic state around 121.43 K and under a 5 T magnetic field change, the magnetic entropy change was calculated to be $0.28 \text{ Jkg}^{-1}\text{K}^{-1}$. The results of this study, particularly the phase transition temperature and magnetic entropy change values, offer valuable insights into the potential of our sample as a candidate for magnetic refrigeration. Further optimization of these parameters could solidify its candidacy.

Keywords: Magnetic cooling systems, Refrigerants, Magnetocaloric effect, Double perovskite, A-site substitution

Copyright © 2024 by author(s), DergiPark and JOEBS. This work is licensed under the Creative Commons Attribution International License (CC BY 4.0).

[CC BY 4.0 Deed | Attribution 4.0 International | Creative Commons](https://creativecommons.org/licenses/by/4.0/)

Received :24.06.2024

Accepted :27.07.2024

How to cite this article: Arda Kandemir, Exploring the effects of Pb substitution on the structure, magnetic, and magnetocaloric properties of $\text{La}_{1.96}\text{Pb}_{0.04}\text{NiMnO}_6$, Journal of Engineering and Basic Sciences, 2024, 02, 1504105

1. INTRODUCTION

Technological advancements, while improving our comfort, present challenges due to increased energy demands and greenhouse gas emissions. This necessitates urgent solutions to protect human health. In response to these challenges, society must explore sustainable solutions. Green technologies with high efficiency are emerging as a promising answer, with the potential to significantly lighten these problems. Due to their high energy consumption rates, refrigeration systems present a main target for efficiency improvements compared to other technologies. They are responsible for approximately 15% (1) of global

*Corresponding author: ardakandemir88@gmail.com

energy use. The enhancement is becoming necessary in these systems due to rising energy demands. Additionally, the current cooling technology has negative impacts such as harmful effects, high costs, low efficiency (2, 3) and these impacts should be resolved. In contrast to these limitations, the alternative technology, magnetic cooling system, offers greener, cheaper, and more effective (4-6). From this aspect, the magnetic cooling system which depends on magnetocaloric effect (MCE) is having the attention of scientists and their research groups as this alternative system offers a potential solution to the current problems mentioned above.

The MCE is a fascinating phenomenon where magnetic materials exhibit temperature changes in response to a varying magnetic field. This temperature change is a key property of these materials and can be quantified by measuring either the adiabatic temperature change or the total magnetic entropy change (4, 6, 7). MCE is the main factor of the MC technology and provides cost reduction, enhancement in efficiency, and environmentally friendly compared to the conventional cooling technology (3-5, 8-11). A critical parameter for MCE is the material's $-\Delta S_M^{max}$, which is the result of the magnetic moment alignment changes of the material and the temperature of its magnetic phase transition. Materials with a large $-\Delta S_M^{max}$ are specifically necessary for magnetic refrigeration. To achieve highly efficient magnetic refrigeration systems with improved MCE performance, researchers are actively exploring various material classes (5, 8, 10, 12-14). The top value of the MCE (15) was achieved by using Gadolinium (Gd) and its alloys/compounds. Moreover, other types of material families have high MCE too and these are the alloys of La-Fe-Si, Ni-Mn-Sn, Mn-As, and Mn-P based materials. Despite their high MCE values, these material classes challenge high cost, potential toxicity, and irreversible cooling cycle (16-18). In contrast, manganite perovskites offer a promising alternative. These materials have several advantages such as chemically stable, cost-effective to produce, and exhibit reversible cooling cycles (5, 10, 12, 19-23). These features make them a good candidate for practical refrigeration applications.

The variation in the perovskite manganite structure, along with the usability of many elements in the periodic table, contributes to a variety of physical properties. The general formula representation of perovskite is $R_{1-x}A_xMnO_3$ where R, and A represent rare and alkaline earth elements, respectively. The less explored subclass of perovskite manganites is double perovskite and can be represented with another formula as $R_xA_{1-x}B_xTM_2O_6$ where R is the rare earth elements, A and B are alkaline earth elements, and TM represents transition metals. R_2BMnO_6 (B for Ni, Co) is also double perovskites which receive attention for usability as a refrigeration application for low temperature due to their huge cooling capacity (24-26). Contrary to their huge cooling capacity, their phase transition

temperature value is low. With appropriate improvements they can be considered an application that works at high temperatures. Using Pb substitution at the A-site of perovskite manganites may contribute to increase in T_C around room temperature (27, 28).

Motivated by the aforementioned, this study investigated the effects of Pb substitution on structure, magnetic, and magnetocaloric features of $La_{1.96}Pb_{0.04}NiMnO_6$ double perovskite manganite system.

2. MATERIALS AND METHODS

For the production of the polycrystalline $La_{1.96}Pb_{0.04}NiMnO_6$ double perovskite manganite the sol-gel method has been selected and the sample labeled as LPNM-004. Using appropriate stoichiometric quantities of $La(NO_3)_3 \cdot 6H_2O$ (99.999% purity, Aldrich), $Pb(NO_3)_2$ ($\geq 99.5\%$ purity, Aldrich), $Ni(NO_3)_2 \cdot 6H_2O$ (99% purity, Merck) and $Mn(NO_3)_2 \cdot xH_2O$ (99.9% purity, Bostonchem) were well mixed with proper pure water separately to form aqueous solutions. Once all aqueous solutions were ready, a single solution was obtained by mixing them together. For sol-gel technique, the solution was prepared using the citric acid monohydrate (CAS Number: 5949-29-1, Aldrich) as a reagent and ethylene glycol ($\geq 99\%$ purity, Aldrich) as the solvent. The solution was continuously stirred at 300 °C, until a dry gel was formed. To remove organic material and obtain metal oxides, two-step process has been followed. First, the dry gel was burned in air at 550 °C for one hour. Afterward calcination was performed at 600 °C in air for six hours. For achieving a homogeneous mixture, the resulting compound was subjected to grinding and mixing process in a Retsch RM 200 mortar grinder for 10 minutes with six repeats. The powder mixture was then pressed into pellets using a hydraulic press (Maassen MP 250). Finally, the pellets were sintered at 1000 °C in air for 24 hours and then allowed to cool down to room temperature.

The crystal structure and phase purity of the sample was investigated using X-ray diffraction (XRD) with $CuK\alpha$ radiation ($\lambda = 1.5406 \text{ \AA}$) at room temperature. The XRD pattern of the sample was examined using the X'Pert High Score Plus software, Fullprof fitting software, and the Rietveld refinement method. The SEM analysis was performed to reveal the structural morphological features of the sample. Energy Dispersive X-Ray Spectroscopy (EDS) is another essential analysis that is used for exposing the elemental composition and their features of the sample. The elemental composition of the sample was analyzed using Energy-Dispersive X-Ray Spectroscopy (EDS). This technique identifies the elements present and their relative abundances in the sample.

The magnetic properties ($M(T)$ for temperature dependence and $M(H)$ for field dependence) of the sample was measured using a Vibration Sample Magnetometer (VSM) within a Physical Properties Measurement System

(PPMS). $M(T)$ was measured in both zero field cooled (ZFC) and field cooled (FC) modes from 10 K to 350 K temperature range. The sample was cooled down to 10 K for ZFC mode without applying any magnetic field. This study utilized Çukurova University Central Research Laboratory (ÇÜMERLAB) for all measurements, analysis, and techniques.

3. Results and Discussion

The crystallographic structure of the sample was researched with XRD analysis, and the data of this analysis has been collected at room temperature. Using Fullprof software (29), the Rietveld's refinement method (30) has been utilized to get the structural result. The graphical view of the result is shown in Figure 1 for LPNM-004 compound. Besides the graph of the result, the parameters of the structure achieved by the refinement analysis can be seen in Table 1.

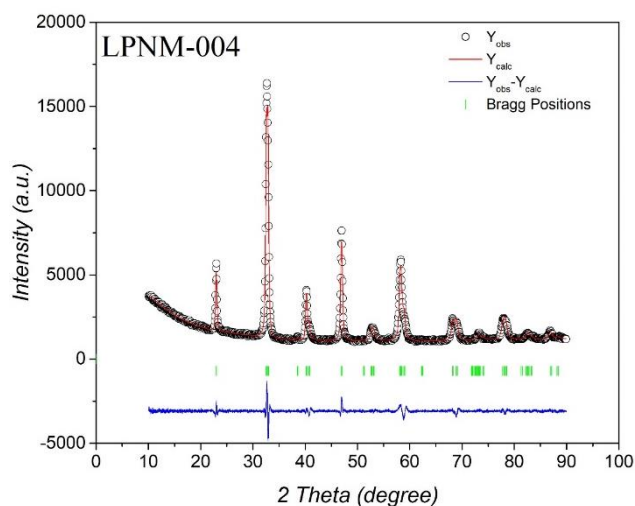


Figure 1. XRD Patterns of LPNM-004. The black circle, red line, blue line, and green bars represent the observed data, calculated data, differences between observed and calculated data, and Bragg positions respectively.

According to XRD patterns and peaks in Figure 1, crystallization has occurred for the sample. The convergence factor (χ^2) value from Rietveld refinement method implies that the theoretical model and the experimental result are consistent with each other. From the analysis, it is seen that the crystal structure of the compound is rhombohedral with $R\bar{3}c$ space group. One of the important factors for the crystal structure is the average ionic radius of the A-site ($\langle r_A \rangle$). It is an arithmetic mean of the ions' ionic radius where they are settled in the A-site of the perovskite crystal structure. The stability and the distortion degree in perovskite structure can be provided by using this parameter.

Another important factor, the Goldschmidt tolerance factor, can tell how the crystal structure changes by the ions

and their radius in the A and B site. The equation to calculate this parameter is:

$$t_G = \frac{\langle r_A \rangle + r_O}{\sqrt{2}(\langle r_B \rangle + r_O)} = 1 \text{ (ideal structure)} \quad (1)$$

where $\langle r_A \rangle$, r_O , and r_B represent the average A-site ionic radius, the ionic radius of oxygen ion, and the ionic radius of Mn and Ni ion, respectively. The low spin value of the ionic radius of Ni^{3+} is selected from the effective ionic radius table (31). The tolerance factor of the sample is close to unity, which means the crystal structure of this perovskite sample is near the ideal crystal structure form. On the other hand, the tolerance factor value shows that there is a distortion in this crystal structure as the value is not 1.00.

Table 1. The structural parameters of LPNM-004 compound. The lattice parameters of the structure (a, b, c, and unit cell volume (V)), the crystal structures with space groups, tolerance factor (t_r), average ionic radius of the A-site, average bond angle of Ni/Mn-O-Ni/Mn, average bond length of Ni/Mn-O, crystallite size (D), size mismatch effect coefficient (σ^2), the bandwidth (W), and convergence factor χ^2 values for the compound.

Structural Parameters	LPNM-004
a (Å)	5.49714
b (Å)	5.49714
c (Å)	13.2845
V (Å ³)	347.6558
Crystal Structure	Rhombohedral
Space Group	$R\bar{3}c$
t_r	0.9968
$\langle r_A \rangle$ (Å)	1.3495
$\langle \text{Ni/Mn-O-Ni/Mn} \rangle$ (°)	162.4434
$\langle d_{\text{Ni/Mn-O}} \rangle$ (Å)	1.9489
D (nm)	18.8074
σ^2 (Å ²)	0.000625
W	0.095620
χ^2	3.21

The size mismatch effect coefficient (σ^2) is another crucial aspect of the crystal structure, and it gives information about the dislocation in the A-site as it is the alteration of the ionic distribution of the A-site. To calculate (σ^2), the equation down below is used:

$$\sigma^2 = \sum_i x_i r_i^2 - \langle r_A \rangle^2 \quad (2)$$

where x_i , r_i , and $\langle r_A \rangle$ denote the fractional occupancy of the i^{th} ion in the A-site, the ionic radii of the corresponding ion in the A-site, and the average ionic radius of the A-site, respectively. The lower the value in the σ^2 , the less electron scatter is in the crystal structure which can help to improve the electronic properties and the conduction of the compound (32, 33).

Furthermore, other key factor influencing in the magnetic properties is the crystallite size (D) which can be calculated by the Debye-Scherrer equation (34, 35):

$$D = \frac{\kappa\lambda}{\beta\cos\theta} \quad (3)$$

where κ , λ , and β symbolize the crystallite shape factor (0.94 for each sample), the wavelength of the x-ray ($\lambda_{\text{Cu-}\kappa\alpha} = 1.5406 \text{ \AA}$), and the peak full width at half maximum at the observed peak angle θ (in radians), respectively.

Worth noting is the role of the e_g electron bandwidth (W) in understanding the magnetic and electronic properties of the substituted manganites. The formula for W is given by:

$$W = \cos\left(\frac{1}{2}[\pi - \langle\theta_{\text{Ni/Mn-O-Ni/Mn}}\rangle]\right) / \langle R_{\text{Ni/Mn-O}} \rangle^{3.5} \quad (4)$$

where the θ and R represents the bond angle and bond length, respectively. W has a stronger influence on ferromagnetism and metallic behavior in magnetic materials. Materials with higher W tend to have higher Curie temperature, metal-insulator transition temperatures, and lower resistivity (ρ). W exhibits proportionality to the t parameter, which quantifies the inter-site hopping interaction of the e_g electrons. This effect is caused by the movement of d electrons between neighboring B-sites. This movement, called super-transfer, involves the electrons occupying oxygen (O) 2p orbitals (36).

The SEM and EDS analysis has been carried out to understand the morphological and elemental features of the sample. The SEM micrograph and EDS spectra graph of the sample have been combined and given in Figure 2.

According to SEM micrograph, polygonal shapes with different sizes are available and the grain structural shapes are homogeneous with a high percentage.

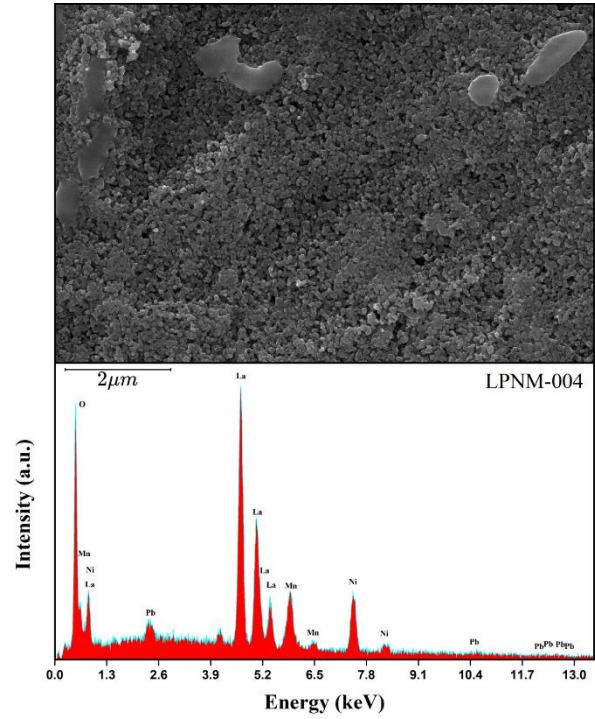


Figure 2. Analysis of SEM and EDS for LPNM-004.

The grain boundaries are visible and few liquid phase features (37) in the structure can induce grain agglomeration, potentially impacting the physical properties of the compound, particularly their magnetic behavior.

For understanding the elemental composition of the sample, EDS spectra has been used and the EDS analysis revealed that stoichiometry is maintained throughout the preparation and heat treatment of the sample which means there is no change in the elemental ratios compared to the starting elements. In addition to stoichiometry, EDS analysis shows that there is no impurity in the sample. This is clear evidence that the sample has been produced successfully without involving any unwanted elements.

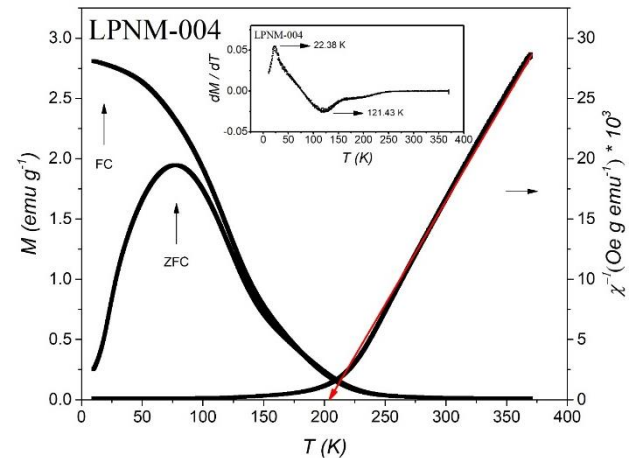


Figure 3. The magnetization measurement with FC and ZFC modes and the inverse susceptibility determined with respect to the temperature for LPNM-004.

The magnetic and magnetocaloric features of the sample are as important as the crystal structure. For the magnetic behavior of the compound, the graph of the temperature-dependent magnetization curves and the inverse susceptibility for the sample are shown on a graph with dual Y-axes in Figure 3. The left axis represents the magnetization values $M(T)$ measured in both FC and ZFC modes. Both modes worked under 25 mT applied magnetic field. Magnetization gradually decreases with increasing temperature, indicating a Ferromagnetic (FM) to the Paramagnetic (PM) phase transition. Below the Curie temperature, the sample shows reversible magnetic behavior in FC and ZFC measurements. This reversibility might be due to a combination of factors like canted spins, domain wall pinning effect, and magnetic anisotropy (38-41). The Curie temperature value can be determined by the point where the FC and ZFC magnetization curves split each other as it is known as the magnetic phase transition temperature. Additionally, the magnetic phase transition temperature can be observed in the inset to Figure 3 ($dM/dT - T$ graph) and its numerical value is tabulated in Table 2. For the low-temperature section, maximum split and cusps were observed and it can be related to the blocking temperature (42, 43). This may point out the spin-cluster metastable or spin-glass-like states. Above T_C value, the inverse susceptibility versus temperature graph in Figure 3 (right axis) demonstrates approximately linear and can be fitted to Curie-Weiss law.

Table 2. The magnetic and magnetocaloric parameters for LPNM-004 and some studied samples from literature.

Sample	Ref.	T_C (K)	μ_{eff} (μ_B)	$-\Delta S_M$ ($J\ kg^{-1}K^{-1}$)	RCP ($J\ kg^{-1}K^{-1}$)
LPNM-004	C.W	121.43	11.71	0.28	N/A
(La _{0.9} Dy _{0.1}) _{0.9} Pb _{0.1} MnO ₃	(27)	172	N/A	0.74	~50
(La _{0.9} Dy _{0.1}) _{0.8} Pb _{0.2} MnO ₃	(27)	249	N/A	1.1	~50
(La _{0.9} Dy _{0.1}) _{0.7} Pb _{0.3} MnO ₃	(27)	322	N/A	1.06	~50
PrSr _{0.9} Pb _{0.1} Mn ₂ O ₆	(28)	274	3.79	0.34	241
PrSr _{0.9} Pb _{0.1} Mn ₂ O ₆	(28)	282	3.90	0.32	311
PrSr _{0.9} Pb _{0.1} Mn ₂ O ₆	(28)	286	4.09	0.42	246

*C.W Current Work

The Curie-Weiss law relation can be given as:

$$\chi = \frac{C}{T - \theta} \quad (5)$$

where C , and θ parameters represent, the Curie constant and the paramagnetic curie temperature, respectively. The mathematical expression of the C value can be calculated by:

$$C = \frac{N\mu_{eff}^2\mu_B^2}{3k} \quad (6)$$

where N , μ_{eff} , μ_B , k_B express, Avogadro's number, the effective magnetic moment, the Bohr magneton, and Boltzmann constant, respectively. The effective magnetic moment value was determined using the Curie-Weiss Law and the slope obtained from the $M-T$ graph in Figure 3. The μ_{eff} value is given in Table 2 (21, 44).

A key consequence of the applied field is the spontaneous magnetization of the compound. Isothermal magnetization, $M(H)$, was measured for the compound up to a magnetic field of 5 T in the phase transition temperature zone to quantify this effect. The graphical representation of the spontaneous magnetization is given in Figure 4. The temperature difference between each consecutive isothermal $M(H)$ curve is 4 K.

When analyzing the $M(H)$ curves, it is observed that the spontaneous magnetization increases significantly upon application of a small magnetic field at low temperatures which is below T_C . As the magnetic field is further increased, it continues to increase the magnetization level, but it doesn't reach saturation.

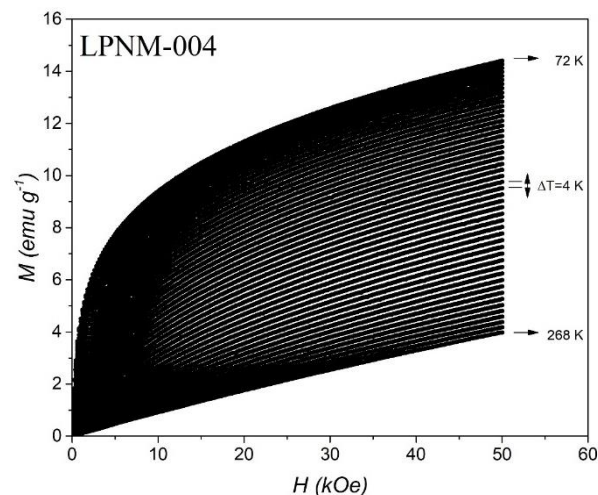


Figure 4. Applied magnetic field dependence of the magnetization curves measured at various temperatures near critical point (T_C) in steps of 4 K for LPNM-004

The limitations in reaching saturation could be attributed to short-range FM interactions, inhomogeneity in the magnetic features, and the presence of FM clusters within the material (45). Beyond the T_C , the material exhibits roughly linear behavior in the magnetization curves, indicating its paramagnetic nature caused by the random orientation of magnetic moments due to thermal energy. Based on the properties observed in the $M(H)$ analysis, the sample displays a transition from the FM to PM phase.

Another key aspect of the magnetocaloric effect is the magnetic entropy change ($-\Delta S_M$), which represents the change in disorder or randomness within the arrangement of magnetic moments. With $-\Delta S_M$, we can measure a magnetocaloric material's cooling potential and it can be calculated using equations:

$$-\Delta S_M = \Delta S_M(T, H) - \Delta S_M(T, 0) = \int_0^H \left(\frac{\partial S}{\partial H} \right)_T dH \quad (8)$$

From Maxwell's thermodynamic relation,

$$\left(\frac{\partial M}{\partial T} \right)_H = \left(\frac{\partial S}{\partial H} \right)_T \quad (9)$$

The equation can be represented as:

$$-\Delta S_M = \int_0^H \left(\frac{\partial M}{\partial T} \right)_H dT \quad (10)$$

Since the experimental data is discrete, the integral calculation can be employed to (9):

$$-\Delta S_M = \sum_i \frac{M_i - M_{i+1}}{T_{i+1} - T_i} \Delta H_i \quad (11)$$

The area under consecutive isothermal magnetization curves from $M(H)$ was used to determine the $-\Delta S_M(T)$ values using the provided equations. The calculated values were presented visually in Figure 5 and numerically in Table 2.

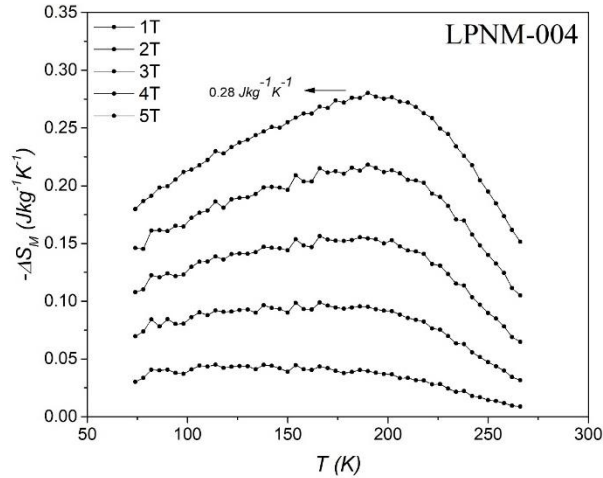


Figure 5. The magnetic entropy change with temperature ($-\Delta S_M(T)$) for LPNM-004.

A number of elements can play a role in determining the $-\Delta S_M$ value of a sample (20). One important factor that can affect $-\Delta S_M$ value of a sample is the double exchange interaction, which is crucial for the material's ferromagnetic features. The $-\Delta S_M$ value of a compound depends on several factors, one of which is how strongly its magnetic moment alignment. This alignment for ferromagnetism is heavily influenced by the double exchange interaction.

By using $-\Delta S_M(T)$ curves, the Relative cooling power (RCP) of the sample can be determined. The RCP value reflects how well the material can transfer the heat, making it a critical parameter for evaluating its MCE. The

RCP value can be calculated using the equation down below:

$$RCP = -\Delta S_M^{max} \times \delta T_{FWHM} \quad (12)$$

where δT_{FWHM} is the full width at the half maximum of the $-\Delta S_M(T)$ curve. RCP measures how much heat a material can move between hot and cold storages in an ideal thermodynamic cycle of magnetocaloric applications. The RCP value for studied sample is given as N/A in Table 2. Since the $-\Delta S_M$ graph in Figure 5 doesn't follow a complete Gaussian distribution, the RCP value couldn't be determined for this compound. This is because the required temperature range falls outside the range of the PPMS equipment.

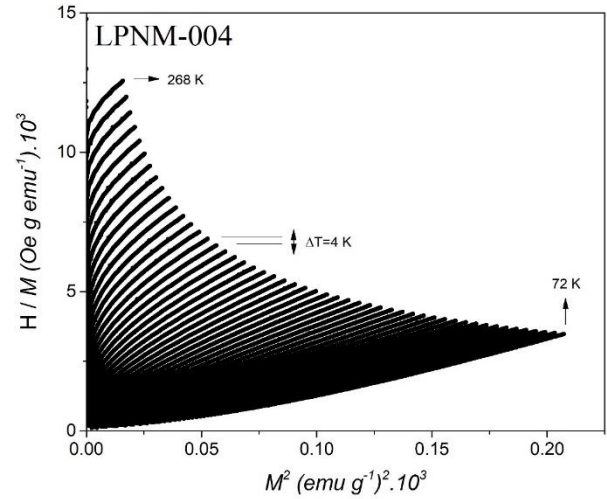


Figure 6. Arrott graph for LPNM-004.

Determining the suitability of a material for magnetic refrigeration also relies on the magnetic phase transition order. Materials with a first-order transition exhibit high thermal and magnetic hysteresis, making them less desirable. Conversely, materials with a second-order transition demonstrate smaller hysteresis and are better candidates. Banerjee's criterion (46), analyzed through the Arrott plot shown in Figure 6, helps us identify the phase transition order.

By analyzing the slopes of the curves in Figure 6, we can determine the material's magnetic phase transition order. A negative slope indicates a first-order magnetic transition, while a positive slope suggests a second-order magnetic transition. The positive slopes in Figure 6 show a second-order magnetic transition for the compound. This is advantageous for magnetic refrigeration since it corresponds to a reversible MCE, making the material more suitable for practical applications.

4. CONCLUSION

The magnetic, magnetocaloric and the structural properties of the LPNM-004 double perovskite compound have been studied and sol-gel technique was selected to produce the compound. According to XRD analysis results, the compound has rhombohedral crystal structure with a

$R\bar{3}c$ symmetry without any impurity phase. From magnetic measurements ($M(T)$ and $M(H)$), the compound exhibits magnetic phase transition from FM to PM and the T_C value is 121.43 K. Using isothermal magnetization curves the $-\Delta S_M$ were calculated, and its value found as $0.28 \text{ Jkg}^{-1}\text{K}^{-1}$ under the 5 T applied magnetic field. Additionally, the Arrott graph revealed a second-order magnetic phase transition from FM to PM at T_C . In the light of the results given above suggests that the produced sample is suitable for magnetic cooling systems operating at low-temperature values. For developing an efficient magnetocaloric refrigeration system for room temperature applications and achieve the level of the results in the literature, more research is essential to modify the composition and enhance the $-\Delta S_M$ value while shifting the phase transition temperature to around room temperature value.

REFERENCES

1. Tassou SA, Ge Y, Hadawey A, Marriott D. Energy consumption and conservation in food retailing. *Applied Thermal Engineering*. 2011;31(2):147-56.
2. Gschneidner Jr KA, Pecharsky VK, Pecharsky AO, Zimm CB. Recent Developments in Magnetic Refrigeration. *Materials Science Forum*. 1999;315-317:69-76.
3. Ayaş AO, Akyol M, Ekicibil A. Structural and magnetic properties with large reversible magnetocaloric effect in $(\text{La}_{1-x}\text{Pr}_x)_{0.85}\text{Ag}_{0.15}\text{MnO}_3$ ($0.0 \leq x \leq 0.5$) compounds. *Philosophical Magazine*. 2016;96(10):922-37.
4. Gschneidner KA, Pecharsky VK. Recent developments in magnetic refrigeration. 1996:209-21.
5. Phan M-H, Yu S-C. Review of the magnetocaloric effect in manganite materials. *Journal of Magnetism and Magnetic Materials*. 2007;308(2):325-40.
6. Gutfleisch O, Willard MA, Brück E, Chen CH, Sankar SG, Liu JP. Magnetic Materials and Devices for the 21st Century: Stronger, Lighter, and More Energy Efficient. 2011;23(7):821-42.
7. Zhang Y, Tian Y, Zhang Z, Jia Y, Zhang B, Jiang M, et al. Magnetic properties and giant cryogenic magnetocaloric effect in B-site ordered antiferromagnetic $\text{Gd}_2\text{MgTiO}_6$ double perovskite oxide. *Acta Materialia*. 2022;226:117669.
8. Gschneidner KA, Pecharsky VK. Magnetocaloric Materials. *Annual Review of Materials Science*. 2000;30(1):387-429.
9. Ayaş AO, Kılıç Çetin S, Akyol M, Akça G, Ekicibil A. Effect of B site partial Ru substitution on structural magnetic and magnetocaloric properties in $\text{La}_{0.7}\text{Pb}_{0.3}\text{Mn}_{1-x}\text{Ru}_x\text{O}_3$ ($x = 0.0, 0.1$ and 0.2) perovskite system. *Journal of Molecular Structure*. 2020;1200:127120-.
10. Ayaş AO, Çetin SK, Akça G, Akyol M, Ekicibil A. Magnetic refrigeration: Current progress in magnetocaloric properties of perovskite manganite materials. *Materials Today Communications*. 2023;35:105988.
11. Kandemir A, Akça G, Kılıç Çetin S, Ayaş AO, Akyol M, Ekicibil A. Effects of Ca substitution on magnetic and magnetocaloric properties in $\text{PrBa}_{1-x}\text{Ca}_x\text{Mn}_2\text{O}_6$ system. *Journal of Solid State Chemistry*. 2023;324:124086.
12. Ram NR, Prakash M, Naresh U, Kumar NS, Sarma TS, Subbarao T, et al. Review on Magnetocaloric Effect and Materials. *Journal of Superconductivity and Novel Magnetism*. 2018;31(7):1971-9.
13. Franco V, Blázquez JS, Ipus JJ, Law JY, Moreno-Ramírez LM, Conde A. Magnetocaloric effect: From materials research to refrigeration devices. *Progress in Materials Science*. 2018;93:112-232.
14. Lyubina J. Magnetocaloric materials for energy efficient cooling. *Journal of Physics D: Applied Physics*. 2017;50(5):53002-.
15. Pecharsky VK, Gschneidner K. A, Jr. Giant Magnetocaloric Effect in $\text{Gd}_5(\text{Si}_2\text{Ge}_2)$. *Physical Review Letters*. 1997;78(23):4494-7.
16. Kim YK, Cho YW. Magnetic transition of $(\text{MnFe}_y\text{P}_{1-x}\text{As}_x)$ prepared by mechanochemical reaction and post-annealing. *Journal of Alloys and Compounds*. 2005;394(1-2):19-23.
17. Shah IA, ul Hassan N, keremu A, Riaz S, Naseem S, Xu F, et al. Realization of Magnetostructural Transition and Magnetocaloric Properties of Ni–Mn–Mo–Sn Heusler Alloys. *Journal of Superconductivity and Novel Magnetism*. 2018;32(3):659-65.
18. Lyubina J, Schafer R, Martin N, Schultz L, Gutfleisch O. Novel design of $\text{La}(\text{Fe},\text{Si})_{13}$ alloys towards high magnetic refrigeration performance. *Adv Mater*. 2010;22(33):3735-9.
19. Barman A, Kar-Narayan S, Mukherjee D. Caloric Effects in Perovskite Oxides. *Advanced Materials Interfaces*. 2019;6(15):1900291-.
20. Zhong W, Au C-T, Du Y-W. Review of magnetocaloric effect in perovskite-type oxides. *Chinese Physics B*. 2013;22(5):57501-.
21. Srivastava SK, Samantaray B, Bora T, Ravi S. Magnetic and electrical properties of Mn-substituted $(\text{La}_{0.85}\text{Ag}_{0.15})\text{CoO}_3$ compounds. *Journal of Magnetism and Magnetic Materials*. 2019;474:605-12.
22. Srivastava SK, Ravi S. Magnetic properties of $\text{Nd}_{1-x}\text{Ag}_x\text{MnO}_3$ compounds. *Journal of Physics: Condensed Matter*. 2008;20(50).
23. Srivastava SK, Kar M, Ravi S, Mishra PK, Babu PD. Magnetic properties of electron-doped $\text{Y}_{1-x}\text{Ce}_x\text{MnO}_3$ compounds. *Journal of Magnetism and Magnetic Materials*. 2008;320(19):2382-6.
24. Krishna Murthy J, Devi Chandrasekhar K, Mahana S, Topwal D, Venimadhav A. Giant magnetocaloric effect in $\text{Gd}_2\text{NiMnO}_6$ and

- Gd₂CoMnO₆ ferromagnetic insulators. *Journal of Physics D: Applied Physics*. 2015;48(35):355001-.
25. Moon JY, Kim MK, Choi YJ, Lee N. Giant Anisotropic Magnetocaloric Effect in Double-perovskite Gd₂CoMnO₆ Single Crystals. *Scientific Reports*. 2017;7(1):16099-.
 26. Moon JY, Kim MK, Oh DG, Kim JH, Shin HJ, Choi YJ, et al. Anisotropic magnetic properties and giant rotating magnetocaloric effect in double-perovskite Tb₂CoMnO₆. *Physical Review B*. 2018;98(17):174424-.
 27. Ho TA, Thanh TD, Thang PD, Lee JS, Phan TL, Yu SC. Magnetic Properties and Magnetocaloric Effect in Pb-Doped La_{0.9}Dy_{0.1}MnO₃ Manganites. *IEEE Transactions on Magnetics*. 2014;50(6):1-4.
 28. Ayaş AO. Structural and magnetic properties with reversible magnetocaloric effect in PrSr_{1-x}Pb_xMn₂O₆ (0.1 ≤ x ≤ 0.3) double perovskite manganite structures. *Philosophical Magazine*. 2018;98(30):2782-96.
 29. Rodríguez-Carvajal J. Recent advances in magnetic structure determination by neutron powder diffraction. *Physica B: Condensed Matter*. 1993;192(1):55-69.
 30. Rietveld H. A profile refinement method for nuclear and magnetic structures. *Journal of Applied Crystallography*. 1969;2(2):65-71.
 31. Shannon RD. Revised effective ionic radii and systematic studies of interatomic distances in halides and chalcogenides. *Acta Crystallographica Section A*. 1976;32(5):751-67.
 32. Soylu Koc N, Altintas SP, Mahamdioua N, Terzioglu C. Cation size mismatch effect in (La_{1-y}RE_y)_{1.4}Ca_{1.6}Mn₂O₇ perovskite manganites. *Journal of Alloys and Compounds*. 2019;797:471-6.
 33. Venkataiah G, Prasad V, Venugopal Reddy P. Influence of A-site cation mismatch on structural, magnetic and electrical properties of lanthanum manganites. *Journal of Alloys and Compounds*. 2007;429(1):1-9.
 34. Debye P, Scherrer P. Interference on inordinate orientated particles in roentgen light. *Physikalische Zeitschrift*. 1916;17:277-83.
 35. Debye P, Scherrer P. Interference on inordinate orientated particles in x-ray light. III. *Physikalische Zeitschrift*. 1917;18:291-301.
 36. Tokura Y. Critical features of colossal magnetoresistive manganites. *Reports on Progress in Physics*. 2006;69(3):797-851.
 37. Koc R, Anderson HU. Liquid phase sintering of LaCrO₃. *Journal of the European Ceramic Society*. 1992;9(4):285-92.
 38. Debnath JC, Zeng R, Kim JH, Shamba P, Chen DP, Dou SX. Effect of frozen spin on the magnetocaloric property of La_{0.7}Ca_{0.3}CoO₃ polycrystalline and single crystal samples. *Journal of Alloys and Compounds*. 2012;510(1):125-33.
 39. Kılıç Çetin S, Acet M, Ekicibil A. Effect of Pr-substitution on the structural, magnetic and magnetocaloric properties of (La_{1-x}Pr_x)_{0.67}Pb_{0.33}MnO₃ (0.0 ≤ x ≤ 0.3) manganites. *Journal of Alloys and Compounds*. 2017;727:1253-62.
 40. Taşarkuyu E, Coşkun A, Irmak AE, Aktürk S, Ünlü G, Samancıoğlu Y, et al. Effect of high temperature sintering on the structural and the magnetic properties of La_{1.4}Ca_{1.6}Mn₂O₇. *Journal of Alloys and Compounds*. 2011;509(9):3717-22.
 41. Yang J, Song WH, Ma YQ, Zhang RL, Zhao BC, Sheng ZG, et al. Structural, magnetic, and transport properties in the Pr-doped manganites La_{0.9-x}Pr_xTe_{0.1}MnO₃ (0 ≤ x ≤ 0.9). *Physical Review B*. 2004;70(14):144421-.
 42. Rana DS, Kuberkar DG, Malik SK. Field-induced abrupt change in magnetization of the manganite compounds (La_R)_{0.45}(CaSr)_{0.55}MnO₃ (R = Eu and Tb). *Physical Review B*. 2006;73(6):064407.
 43. Bourouina M, Krichene A, Chniba Boudjada N, Boujelben W. Structural disorder effect on the structural and magnetic properties of Pr_{0.4}Re_{0.1}Sr_{0.5-y}BayMnO₃ manganites (Re = Pr, Sm, Eu, Gd, Dy and Ho). 2017;43(15):12311-20.
 44. Mugiraneza S, Hallas AM. Tutorial: a beginner's guide to interpreting magnetic susceptibility data with the Curie-Weiss law. *Communications Physics*. 2022;5(1):95.
 45. Phong PT, Dang NV, Bau LV, An NM, Lee I-J. Landau mean-field analysis and estimation of the spontaneous magnetization from magnetic entropy change in La_{0.7}Sr_{0.3}MnO₃ and La_{0.7}Sr_{0.3}Mn_{0.95}Ti_{0.05}O₃. *Journal of Alloys and Compounds*. 2017;698(C):451-9.
 46. Banerjee BK. On a generalised approach to first and second order magnetic transitions. *Physics Letters*. 1964;12(1):16-7.